Endo-lysosomal sorting and degradation of Tau mediates glucocorticoid-driven hippocampal malfunction

João Vaz-Silva[1,2,3], Mei Zhu[3], Qi Jin[3], Viktoriya Zhuravleva[3], Patrícia Gomes[1,2], Sebastian Quintremil[3], Torcato Meira[1,2,4], Joana Silva[1,2], Chrysoula Dioli[1,2] Carina Soares-Cunha[1,2], Nikolaos P. Daskalakis[5], Nuno Sousa[1,2], Ioannis Sotiropoulos[1,2, ‡], Clarissa L Waites[3, ‡ *]

[1] Life and Health Sciences Research Institute (ICVS), School of Medicine, University of Minho, Campus de Gualtar, 4710-057, Braga, Portugal

[2] ICVS/3B's - PT Government Associate Laboratory, Braga/Guimarães, 4710-057, Portugal

[3] Department of Pathology and Cell Biology, Taub Institute for Research on Alzheimer's Disease and the Aging Brain, Columbia University Medical Center, New York, New York 10032, USA.

[4] Department of Neuroscience, Columbia University, New York, NY 10032, USA

[5] Deparment of Psychiatry, McLean Hospital, Harvard Medical School, Belmont, MA 02478, USA.

[‡]contributed equally

[*]corresponding author: Clarissa Waites, Department of Pathology and Cell Biology, Taub Institute for Research on Alzheimer's Disease and the Aging Brain, Columbia University Medical Center, New York, New York 10032, USA

Abstract (175 words)

Emerging studies implicate Tau as an essential mediator of neuronal atrophy and cognitive impairment in Alzheimer's disease (AD), yet the factors that precipitate Tau dysfunction in AD are poorly understood. Chronic environmental stress and elevated glucocorticoids (GC), the major stress hormones, are associated with increased risk of AD, and have been shown to trigger intracellular Tau accumulation and downstream Tau-dependent neuronal dysfunction. However, the mechanisms through which stress and GC disrupt Tau clearance and degradation in neurons remain unclear. Here, we demonstrate that Tau undergoes degradation via endo-lysosomal sorting in a pathway requiring the small GTPase Rab35 and the endosomal sorting complex required for transport (ESCRT) machinery. Furthermore, we find that GC impair Tau degradation by decreasing Rab35 levels, and that AAV-mediated expression of Rab35 in the hippocampus rescues GC-induced Tau accumulation and related neurostructural deficits. These studies indicate that the Rab35/ESCRT pathway is essential for Tau clearance and part of the mechanism through which GC precipitate brain pathology.

Introduction

Intraneuronal accumulation of Tau protein represents a central pathogenic process in Alzheimer's disease (AD), and is hypothesized to mediate the detrimental effects of amyloid-beta (Aβ) on neuronal function and cognitive performance[1-3]. Tau accumulation and hyperphosphorylation is linked to synaptic atrophy, neuronal dysfunction, and cognitive deficits[4,5], and triggers these events by disrupting axonal trafficking[6], promoting GluN2B-related excitotoxicity[2,7], and suppressing nuclear CREB-mediated synthesis of synapse- and memory-related proteins[5], among other effects. Furthermore, emerging studies support a crucial role for Tau in diverse brain pathologies (for review, see [8]) including prolonged exposure to stressful conditions, a known risk factor for AD and major depressive disorder [9]. In particular, recent studies demonstrate that exposure to chronic environmental

stress or the major stress hormones, glucocorticoids (GC), triggers the accumulation of Tau and its synaptic missorting, precipitating dendritic atrophy and synaptic dysfunction in a Tau-dependent manner[10-14]. However, the cellular mechanisms responsible for stress/GC-induced accumulation of Tau remain unclear.

A major cause of Tau accumulation is the dysfunction of its degradative pathways[15]. Tau degradation has been shown to occur through two distinct mechanisms, the ubiquitin-proteasome system and the autophagy-lysosome pathway[16,17]. Indeed, proteasome and lysosome inhibitors can delay Tau turnover and promote Tau-driven neuropathology[18,19]. However, dysfunction of a third degradative pathway, the endo-lysosomal system, is also linked to AD and other neurodegenerative conditions that exhibit Tau accumulation, including Parkinson's disease [20-22]. Nevertheless, the role of the endo-lysosomal pathway in the clearance of Tau is almost completely unexplored.

Here, we report that the small GTPase Rab35 and the endosomal sorting complex required for transport (ESCRT) machinery mediate the delivery of Tau to lysosomes via early endosomes and multivesicular bodies (MVBs). We further demonstrate that this pathway is negatively regulated by GCs, which suppress Rab35 transcription, thereby inhibiting Tau degradation and promoting its accumulation. Finally, we show that *in vitro* and *in vivo* overexpression of Rab35 can rescue GC-induced Tau accumulation and neurostructural deficits in hippocampal neurons. These findings demonstrate Rab35's critical role as a regulator of Tau clearance under physiological and pathological conditions.

Results

The ESCRT pathway is necessary and sufficient for Tau degradation

Despite its primarily axonal and microtubule-related distribution, Tau is also found in the somatodendritic compartment and associated with lipid membranes[23,24]. To determine whether Tau

undergoes endosomal sorting, we looked for Tau immunoreactivity in multivesicular bodies (MVBs), late endosomal structures that deliver cargo to lysosomes. Immuno-electron microscopy in rat hippocampal tissue revealed MVBs that contain Tau immunogold labeling (Fig. 1A; Fig. S1A), indicating that Tau is sorted into MVBs and can potentially undergo degradation via the endocytic pathway. MVB biogenesis is catalyzed by the endosomal sorting complex required for transport (ESCRT) system, a series of protein complexes that recruit ubiquitylated cargo destined for degradation and facilitate the formation of intralumenal vesicles[25]. The initial component of the ESCRT complex, Hrs, is essential for binding and recruitment of ubiquitylated cargo into MVBs[25,26]. To examine whether Hrs interacts with Tau, we performed the proximity ligation assay (PLA; see Fig. 1B) in N2a cells overexpressing mCh-tagged Hrs (Fig. 1C; Fig. S1B). Here, we detected fluorescent puncta, representing close (20-50 nm) proximity of Hrs and Tau, that were associated with Hrs-positive early endosomes (Fig. 1C) and increased upon overexpression of GFP-tagged wild-type Tau (GFP-wtTau; 4R0N isoform[27])(Fig. S1B,D), demonstrating specificity of the PLA signal for the Hrs/Tau interaction. This interaction was confirmed by co-immunoprecipitation (IP) experiments in N2a cells overexpressing FLAG-Hrs and either GFP or GFP-wtTau, wherein Hrs was specifically pulled down by GFP-wtTau (Fig. S1E). Treatment with a deubiquitylating enzyme (DUB) inhibitor to increase ubiquitylated Tau species further increased the Hrs/Tau interaction as measured by both co-IP and PLA (Fig. S2A-D), indicating that ubiquitylation promotes Tau's association with Hrs and subsequent entry into ESCRT pathway. Using high resolution fluorescence microscopy, we also identified Tau in both membranes and lumen of Hrs-, EEA1-, and Rab5-positive early endosomes in N2a cells (Fig. 1D-E). These findings demonstrate the presence of Tau in endosomal compartments at both early and late stages of the endo-lysosomal pathway.

Rab35 promotes Tau degradation through the ESCRT pathway

To assess the role of the ESCRT pathway in Tau clearance (Fig. 2A), we measured Tau degradation in primary hippocampal neurons lentivirally transduced with an shRNA against TSG101, an essential component of the ESCRT-I complex. Depletion of TSG101 is a common mechanism for blocking degradation of ESCRT pathway cargo [28,29], and our shTSG101 hairpin reliably reduces TSG101 levels by ~60% (Fig. 2D). Using a previously-described cycloheximide (CHX)-chase assay to measure the fold-change in Tau degradation[30], we found that shTSG101 decreased this value by 30% (Fig. 2B-C), indicating its ability to inhibit Tau degradation. Conversely, activation of the ESCRT pathway by TSG101 overexpression increased Tau degradation by ~30% (Fig. 2E-F). Together, these findings indicate that the ESCRT pathway is both necessary and sufficient for mediating Tau degradation.

In recent work, we demonstrated that ESCRT-0 protein Hrs is an effector of the small GTPase Rab35, and is recruited by active Rab35 to catalyze downstream ESCRT recruitment and MVB formation[30]. Therefore, we investigated whether Rab35 is also a key regulator of Tau degradation. Again using the CHX-chase assay, we measured Tau degradation in neurons transduced with a previously-characterized shRNA to knockdown Rab35 (shRab35; Fig. 2I)[30]. We found that shRab35 decreased Tau degradation by ~30% (Fig. 2G-H), indicative of Rab35's role in this process. Moreover, overexpression/gain-of-function of mCherry-tagged Rab35 increased Tau degradation by nearly 50% compared to mCh control (Fig. 2J-K), demonstrating that Rab35 is a potent regulator of Tau turnover.

We further confirmed the effect of Rab35 on Tau with a flow cytometry assay using N2a cells transfected with HA-Rab35 and medium fluorescent timer (FT)-tagged wild-type Tau. The emission of medium FT changes from blue to red as it matures, with half-maximal red fluorescence at 3.9 hours (Fig. 2L)[31], and this fluorophore has previously been used to monitor protein degradation based on the intensities of red ("older") vs. blue ("younger") fluorescent protein in cells[32]. We found that the ratio of red:blue (old:new) FT-wtTau was significantly lower in N2a cells co-expressing HA-Rab35 compared to HA vector control (Fig. 2M), indicating faster Tau degradation. Rab35 overexpression

did not alter the red:blue ratio when FT alone was expressed in N2a cells (Fig. S3A), confirming that Rab35 specifically stimulates Tau degradation. Given that Tau hyperphosphorylation is a key pathogenic event in AD and other tauopathies[3], we also evaluated whether Rab35 could stimulate the degradation of hyperphosphorylated Tau, using the phospho-mimetic E14 Tau mutant, in which 14 serine and threonine residues are replaced with glutamic acid[27]. The ratio of red:blue FT-E14Tau was again significantly lower in HA-Rab35-expressing N2a cells (Fig. 2N), indicating Rab35's ability to mediate the degradation of phosphorylated Tau.

Since Tau is phosphorylated at multiple sites, we used antibodies against several phospho-Tau epitopes (PHF1, Ser262, CP13) to determine which Tau species were sensitive to Rab35/ESCRT-mediated degradation. Interestingly, we found that degradation of both PHF1 and Ser262 phospho-Tau species (measured by CHX-chase assay) were significantly slowed by knockdown of Rab35, while CP13 phospho-Tau was unaffected (Fig. 3A-B). We saw similar results with knockdown of Tsg101 (Fig. S3B-C). To further verify that Rab35 stimulates Tau degradation through the ESCRT pathway, we assessed the effect of Rab35 on Hrs/Tau interaction by PLA. Here, N2a cells were co-transfected with FLAG-Hrs and mCherry or mCh-Rab35, and PLA performed with antibodies against FLAG and either total or phospho-Tau (PHF1, Ser262, CP13). For total Tau, as well as PHF1 and Ser262 Tau, Rab35 expression significantly increased the number of fluorescent puncta per cell (Fig. 3C-D), representing increased interaction of these Tau species with Hrs, and thus their subsequent sorting into the ESCRT pathway. In contrast, Rab35 had no effect on PLA puncta number for CP13 Tau (Fig. 3C-D), suggesting that this form of phospho-Tau does not undergo degradation via the Rab35/ESCRT pathway. These PLA data, consistent with our CHX-chase assay findings, suggest that Rab35 promotes the degradation of total Tau and some, but not all, phospho-Tau species through the ESCRT pathway.

To verify that the Rab35/ESCRT pathway mediates Tau degradation through lysosomes, we treated hippocampal neurons with bafilomycin (to block acidification and trap lysosome contents) in the presence of mCh-tagged TSG101 or Rab35 to stimulate Tau degradation (Fig. 4A). We found that

bafilomycin led to a significant accumulation of Tau in lysosomes of neurons expressing either TSG101 or Rab35 versus mCh control (Fig. 4A-B). Furthermore, through sucrose-based fractionation of primary neurons, we found that Rab35 overexpression increased the fraction of Tau in endosomal/lysosomal (Rab35- and LAMP1-enriched) fractions (Fig. S4), providing further support for the stimulating role of Rab35 on Tau sorting into the endo-lysosomal pathway. We also evaluated the effects of Rab35 gain-of-function on Tau stability in different neuronal compartments, using CHX treatment combined with immunofluorescence microscopy in hippocampal neurons expressing mCh or mCh-Rab35, as previously described[30]. Although both Rab35 and Tau are enriched in axons, Rab35 overexpression reduced Tau fluorescence in both axons and neuronal somata, demonstrating increased Tau degradation and the ability of Rab35 to regulate Tau turnover in distinct neuronal compartments (Fig. 4C-D).

Glucocorticoids decrease Rab35 levels *in vitro* and *in vivo*

Clinical studies suggest that stressful life events and high GC levels are risk factors for AD[33,34], and animal studies demonstrate that prolonged exposure to environmental stress and/or elevated GC levels trigger Tau accumulation[9,11,35]. Based on the above findings identifying the Rab35/ESCRT pathway as a critical regulator of Tau degradation, we next examined whether GC treatment altered the levels of Rab35 or ESCRT pathway proteins. Primary neurons were treated with GC and the levels of ESCRT proteins (Hrs, Tsg101, CHMP2b) and Rab35 measured. Surprisingly, we found that GC treatment selectively reduced Rab35 protein levels without altering the levels of other ESCRT proteins (Fig. 5A-B). GC are known to regulate gene transcription via activation of the Glucocorticoid Receptor (GR), which binds Gluocorticoid Response Elements (GRE) within the promoter regions of genes[9]. We therefore used qPCR to measure Rab35 mRNA levels in hippocampal neurons and N2a cells, and found that GC treatment led to a significant reduction in Rab35 mRNA in both cell types (Fig. 5C).

Consistent with the concept that GC regulate Rab35 transcription, we found that the *Rab35* gene contains 14 non-redundant GREs (Table 1).

We subsequently measured the levels of Rab35 and other endocytic Rab GTPases in the hippocampi of rats that received GC injections for 15 days (Fig. 5D). The hippocampus displays overt lesions in both stress- and Tau-related pathologies, and is one of the earliest brain regions to show signs of neurodegeneration[9]. In line with our *in vitro* findings, Rab35 levels were significantly decreased in GC-injected animals, whereas no other Rab GTPases analyzed were significantly altered as assessed by immunoblot analysis (Fig. 5E-F). We observed a similar decrease in immunofluorescence staining of Rab35 in the dorsal hippocampus of GC-treated animals compared to vehicle-treated control animals (Fig. 5G-H; Fig. S5A). Altogether, these *in vitro* and *in vivo* results suggest that GC specifically decrease Rab35 transcription, leading to reduced mRNA and protein levels in hippocampal neurons.

Rab35 gain-of-function rescues GC-induced Tau accumulation and neurostructural deficits

Based on our findings that Rab35 mediates Tau turnover, and that exposure to high GC levels downregulates Rab35, we hypothesized that Rab35 overexpression could attenuate GC-induced Tau accumulation and related neuronal atrophy[13,36,37]. To test this hypothesis, we performed the CHX-chase assay in hippocampal neurons transduced with either mCh or mCh-Rab35, and treated with GC or vehicle control. As shown in Figure 6, GC treatment reduced Tau degradation in mCherry-expressing neurons, but this effect was completely blocked by Rab35 overexpression (Fig. 6A-B). Similar results were found in N2a cells, where Rab35 overexpression prevented the GC-driven increase in total Tau levels (Fig. S5B-C) and in ubiquitylated Tau species (Fig. S5D-F). Since ubiquitylation is the major signal for cargo sorting into the ESCRT pathway, these findings provide further evidence that Rab35 stimulates the endo-lysosomal sorting of Tau.

Previous studies showed that exposure to stress or high GC levels induced Tau accumulation and synaptic missorting, leading to dendritic atrophy and synaptic loss in animals[11,13], and that these hippocampal deficits were Tau-dependent[10,11]. To test whether Rab35 could protect against these GC-induced effects, we injected middle-aged rats with adeno-associated virus (AAV) to express EGFP or EGFP-Rab35 in hippocampus under control of the CaMKII promoter (Fig. 6C), leading to a ~300% increase in Rab35 levels (Fig. S6B,C). Animals were subsequently treated with GC or vehicle control. Both EGFP and EGFP-Rab35 injected animals displayed similar body mass loss following GC administration, demonstrating a similar response to high GC levels (Fig. S6A). However, in contrast to EGFP animals that exhibited significant GC-induced Tau accumulation in hippocampal synaptosomes, animals expressing EGFP-Rab35 did not show any such accumulation (Fig. 6D, E). Furthermore, using Golgi-based 3D neuronal reconstruction of pyramidal neurons in dorsal hippocampus, we found that GC significantly decreased the length of apical dendrites in the EGFP control group, but not in animals expressing EGFP-Rab35 (Fig. 6F, G). Notably, EGFP-Rab35 expression alone did not alter apical dendritic length (Fig. 6G), and no difference in basal dendrite length was found between the groups (Fig. S6D), consistent with previous work showing selective vulnerability of apical dendrites to GC[11]. We also found that GC treatment led to a significant loss of mature spines and concomitant increase of immature spines in EGFP-expressing animals, but no change in mature or immature spine density in EGFP-Rab35 animals (Fig. 6H; Fig. S6C). GC-induced neuronal atrophy was further confirmed by Sholl analysis, which measures the number of dendritic intersections as a function of their distance from the soma. As shown in Figure 6I-J, GC reduced the number of distal dendritic intersections in neurons expressing EGFP but not EGFP-Rab35. Altogether, these *in vivo* findings indicate that Rab35 overexpression prevents GC-driven neurostructural deficits, implicating Rab35 as an essential regulator of GC-induced neuronal dysfunction.

Discussion

Impairment of Tau proteostasis is linked to neuronal and synaptic dysfunction in AD animal models and patients [1-3]. Given that Tau accumulation appears to drive neurodegenerative processes in AD and other neurological diseases (see also Introduction), there is growing interest in understanding the mechanisms that mediate Tau clearance, and their selectivity for different forms of Tau. Previous studies have shown that Tau degradation can occur through the ubiquitin proteasome system (UPS), but that macroautophagy plays an important role in the catabolism of aggregated/insoluble Tau, which is not accessible to the UPS (for review, see[38]). Recent work indicates that chaperone-mediated autophagy and endosomal microautophagy also contribute differentially to the degradation of wild-type versus pathogenic mutants forms of Tau[39], suggesting that Tau turnover is a complex process regulated by multiple factors and involving distinct degradative pathways.

The current study utilizes *in vitro* and *in vivo* approaches to demonstrate a critical role for the endocytic pathway, and in particular Rab35 and the ESCRT machinery, in the turnover of total Tau and specific phospho-Tau species (see Fig. 7). The ESCRT system mediates the degradation of membrane-associated proteins such as epidermal growth factor receptor[25], but it has also been implicated in the degradation of cytosolic proteins GAPDH and aldolase[40]. These findings are of particular relevance for Tau, which has both cytosolic and membrane-associated pools[23,24], and has been shown to localize to different neuronal subcompartments based on its phosphorylation state[13,27]. The current study reveals that Tau appears in Hrs-, EEA1-, and Rab5-positive early endosomes (on the membrane and in the lumen), intraluminal vesicles of MVBs, and LAMP1-positive vesicles and membrane fractions, demonstrating its trafficking through the entire endo-lysosomal pathway. Moreover, we find that Tau interacts with the initial ESCRT protein Hrs, and that this interaction is strengthened by deubiquitylating enzyme inhibitors, indicating its dependence on Tau ubiquitylation. We also observe that the small GTPase Rab35 is a positive regulator of Tau sorting into the ESCRT pathway. Not only does overexpression of Rab35 stimulate Tau's interaction with Hrs and subsequent lysosomal degradation, but Rab35 knockdown significantly slows Tau degradation. Interestingly,

while Rab35 stimulates the turnover of phospho-mimetic E14 Tau, not all phosphorylated Tau species are equally susceptible to degradation in the Rab35/ESCRT pathway. In particular, we find that PHF1 and Ser262 phospho-Tau species undergo Rab35-mediated degradation, while CP13 does not. Such differences might reflect changes in ubiquitylation and/or endosomal membrane association of the different Tau phospho-proteins, although further work is needed to clarify the relationship between Tau phosphorylation, ubiquitylation, and degradation. We recently showed that Rab35 stimulates the degradation of synaptic vesicle proteins, by mediating the recruitment of Hrs to SV pools in response to neuronal activity[30]; however, our current findings represent the first demonstration of the essential role of Rab35 and the ESCRT pathway in regulating the degradation of total and phospho-Tau species.

Recent evidence suggests that dysfunction of the ESCRT machinery itself is associated with profound cytopathology, as brain-specific deletion of ESCRT components in mice leads to the accumulation of ubiquitylated proteins, impaired endosomal trafficking, and cell death [41,42]. Further, a truncating mutation in ESCRT-III protein CHMP2b causes familial frontotemporal dementia and amyotrophic lateral sclerosis, and at the cellular level induces endo-lysosomal pathway dysfunction and the accumulation of ubiquitylated proteins[43,44]. Together with our findings, the above studies support the importance of the endo-lysosomal pathway, and specifically the ESCRT machinery, in the clearance of ubiquitylated proteins such as Tau. Indeed, abnormalities of the endo-lysosomal pathway, including endosomal enlargement and high levels of lysosomal hydrolases, are reported as the earliest intracellular features of AD [45]. Intriguingly, these same features are present in Niemann-Pick Disease Type C (NPC), an inherited lysosomal storage disorder also characterized by Tau pathology [46]. These shared pathological features of AD and NPC indicate a strong connection between endo-lysosomal dysfunction and Tau accumulation, supporting the importance of this degradative pathway for Tau proteostasis and pathological accumulation.

Multiple cellular pathways are altered by chronic stress, increasing the vulnerability of affected individuals to psychiatric and neurodegenerative diseases such as depression and AD[47,48]. For example,

prolonged exposure to stress or high levels of GC trigger Tau accumulation and hyperphosphorylation, accompanied by synaptic missorting of Tau and neuronal atrophy[13,35-37]. Importantly, Tau is essential for this stress/GC-driven damage, as Tau ablation was found to be neuroprotective[12,14,35]. While previous *in vitro* studies showed that GC reduce Tau turnover [49], the underlying molecular mechanisms were unclear. The current study demonstrates that GC impair Tau degradation by downregulating Rab35, thereby suppressing Tau sorting into the ESCRT pathway and leading to the accumulation of ubiquitylated Tau (Fig. 7). These results support the concept that ubiquitylation, the major signal for cargo sorting into the ESCRT pathway, represents the first line of cellular defense against Tau accumulation and related neuronal malfunction[38,50]. Importantly, we find that Rab35 overexpression blocks Tau accumulation and neuronal atrophy induced by high GC levels. Future studies will clarify the potential interplay between endo-lysosomal machinery and other degradative pathways such as autophagy under stressful/high GC conditions. Our current findings identify the Rab35/ESCRT pathway as a critical regulator of Tau proteostasis, supporting its involvement in the intraneuronal events through which the primary stress hormones, GC, impair neuronal morphology and plasticity in the hippocampus[51]. Based on the emerging significance of endosomal trafficking defects in AD brain pathology[20], Rab35 and the endo-lysosomal pathway deserve further investigation for their therapeutic relevance against Tau-dependent neuronal malfunction and pathology.

Acknowledgments

We thank Dr. Peter Davies (Albert Einstein College of Medicine, NY, USA) for the generous gift of Tau antibodies, Dr. Karen Ashe for pRK5-EGFP-Tau (Addgene plasmid #46904), and Dr. Ed Boyden for pAAV-CAMKIIa-EGFP vector (Addgene plasmid #50469). We also thank Fidel at the Bronx FedEx station for his help in recovering a valuable package. This work was supported by NIH grants R01NS080967 and R21MH104803 to C.L.W., Portuguese Foundation for Science & Technology

(FCT) PhD fellowships to J. Vaz-Silva and T. Meira (PD/BD/105938/2014; PD/BD/113700/2015, respectively), and the following grants to I.S.: FCT Investigator grant IF/01799/2013, the Portuguese North Regional Operational Program (ON.2) under the National Strategic Reference Framework (QREN), through the European Regional Development Fund (FEDER), the Project Estratégico co-funded by FCT (PEst-C/SAU/LA0026/2013) and the European Regional Development Fund COMPETE (FCOMP-01-0124-FEDER-037298) as well as the project NORTE-01-0145-FEDER-000013, supported by the Northern Portugal Regional Operational Programme (NORTE 2020), under the Portugal 2020 Partnership Agreement, through the European Regional Development Fund (FEDER).

Author Contributions

J.V-S., I.S., and C.L.W. designed the research; J.V-S., P.G., S.Q., M.Z., V.Z., T.M., J.S., C.D., C. S-C. and N.D. performed experiments and analyzed data; N.S., I.S., and C.L.W. supervised experiments; J.V-S., I.S., and C.L.W wrote the manuscript.

Declaration of Interests

The authors declare no competing interests.

Methods

Primary neurons and cell lines

Primary neuronal cultures were prepared from E18 Sprague Dawley rat embryos and maintained for 14 DIV before use, as described previously [30]. Neuro2a (N2a) neuroblastoma cells (ATCC CCL-131)

and HEK293T cells (Sigma) were grown in DMEM-GlutaMAX (Invitrogen) with 10% FBS (Atlanta Biological) and Anti-Anti (ThermoFisher) and kept at 37°C in 5% CO2. During dexamethasone treatment in N2a cells, FBS content in the growth media was reduced to 3%.

Pharmacological treatments

Pharmacological agents were used in the following concentrations and time courses: cycloheximide (Calbiochem, 0.2 µg/µl, 24 h or 0.1 µg/µl, 16h), bicuculline (Sigma, 40 µM, 24 h), 4-aminopyridine (Tocris Bioscience, 50 µM, 24 h), bafilomycin A1 (Millipore, 0.1 µM, 5h), dexamethasone (Ratiopharm, 10 µM, 48h), dexamethasone (InvivoGen, 20 µM, 72h), epoxomicin (Sigma, 0.1 µM) PR-619 (LifeSensors, 50 µM).

Lentivirus production, transduction and DNA transfection

DNA constructs were described previously [30], with the exception of pRK5-EGFP-Tau (Addgene plasmid #46904), and pAAV-CAMKIIa-EGFP-Rab35, which was created by subcloning EGFP-Rab35 into the pAAV-CAMKIIa-EGFP vector (Addgene plasmid #50469). Both pAAV-CAMKIIa-EGFP-Rab35 and pAAV-CAMKIIa-EGFP were then packaged into AAV8 serotype by the UNC Gene Therapy Center Vector Core (UNC Chapel Hill). Lentivirus was produced as previously described [30]. Neurons were transduced with 50-150uL of lentiviral supernatant per well (12 well plates) or 10-40 uL per coverslip (24 well plates) either at 3 DIV for shRNA transduction or 10 DIV in gain-of-function experiments. Respective controls were transduced on the same day for all experimental conditions. Neurons were collected for immunoblotting or immunocytochemistry at 14 DIV.

Immunofluorescence Microscopy

Immunofluorescence staining in neurons and N2a cells was performed as previously described [30]. Briefly, cells were fixed with Lorene's Fix (60mM PIPES, 25mM HEPES, 10mM EGTA, 2 mM MgCl2, 0.12 M sucrose, 4% formaldehyde) for 15 min, and primary and secondary antibody incubations were performed in blocking buffer (2% glycine, 2% BSA, 0.2% gelatin, 50mM NH4Cl in 1xPBS) overnight at 4ºC or for 1h at room temperature, respectively. For staining of brain slices, coronal vibratome sections (40 µm) of paraformaldehyde-fixed brains were placed in heated citrate buffer for 15 minutes. Sections were then permeabilized using 0.5% Triton X100 for 30 minutes, followed by 5 minutes blocking with Ultravision Protein Block (Thermoscientific). Primary and secondary antibody were diluted in 0.5% Triton/0.2% BSA/0.5% FBS in 1x PBS and incubation was performed overnight at 4ºC or for 3h at room temperature, respectively. Images were acquired using a Zeiss LSM 800 confocal microscope equipped with Airyscan module, using either a 63x objective (Plan-Apochromat, NA 1.4), for neurons or N2a cell imaging, or a 40x objective (Neofluar, NA 1.4) for imaging of rat brain sections. Primary antibodies are listed in Table S1.

Proximity Ligation Assay

Proximity ligation assay (PLA) was performed in N2a cells according to manufacturer's instructions (Duolink, Sigma). Until the PLA probe incubation step, all manipulations were performed as detailed above for the immunocytochemistry procedure. PLA probes were diluted in blocking solution. The primary antibody pairs used were anti-FLAG (Rabbit; Abcam) and DA9 (anti-Total Tau, Mouse, gift from Peter Davies), anti-mCherry (Rabbit, Biovision) and DA9 (Mouse, Peter Davies). Additionally, a blocking FLAG peptide (Sigma), used at a 100 µg/ml concentration, was included to evaluate the specificity of the technique. All protocol steps were performed at 37ºC in a humidity chamber, except for the washing steps. Coverslips were then mounted using Duolink In situ Mounting Media with DAPI.

Tau immunogold staining and electron microscopy

For electron microscope analysis, rat hippocampi were fixed at 4ºC with 4% PFA, then transferred to 4% PFA/0.8 % gluteraldehyde in 0.1 M of phosphate buffer (PB) for 1 h and afterwards, to 0.1 M PB. Vibratome-cut axial sections of the dorsal hippocampus (300 µm thick) were collected, and CA1 hippocampal area was surgically removed. Tissue was then carefully oriented and embedded in Epon resin and ultrathin sections (500 Å), encompassing the superficial-to-deep axis, were cut onto nickel grids. For Tau-immunogold staining, sections were treated with heated citrate buffer (Thermo Scientific) for 30 min and then by 5% BSA. Grids were incubated overnight with Tau5 primary antibody diluted in 1% BSA in PB, followed by secondary gold antibody. Grids were imaged on a JEOL JEM-1400 transmission electron microscope equipped with a Orious Sc1000 digital camera.

Image analysis

Images were analyzed and processed using the Fiji software. PLA puncta were counted using the Multi-point tool. Fluorescence intensity was measured after performing a Z-projection using the SUM function. For cell bodies, the corrected total cell fluorescence was calculated, by subtracting the average fluorescence of the background of the whole area to the Integrated fluorescence density. For Axons, a mask was created in the mCherry channel, representing the experimental condition, using the same threshold value, and the average fluorescence intensity of the axon was then measure in the other channel.

Coimmunoprecipitacion

For coimmunoprecipitation, N2a cells were transfected with Lipofectamine 3000 according to the manufacturer's protocol (Life Technologies). Cell lysates were collected 48h after transfection, after 3x washes with cold PBS, in Co-IP lysis buffer (0,1% NP-40, 1mM EDTA in 1x PBS) with protease

inhibitor (Roche) and phosphatase inhibitor cocktails II and III (Sigma) and clarified by centrifugation at high speed (10 min, 20,000 rcf). Protein concentration was determined using the BCA protein assay kit (ThermoFisher Scientific) and the same amount of protein was used for each condition. Lysates were pre-cleared using magnetic agarose beads (Chromotek) for 1h at 4ºC. For GFP pull down, lysates were incubated with GFP-Trap Magnetic agarose beads (Chromotek) for 3h at 4ºC. Beads were washed 3 times with co-IP lysis buffer and then eluted using 2x sample buffer (Bio-Rad) and subject to SDS-PAGE immunoblotting as described below.

Western Blotting

For Western Blotting experiments, neurons were collected using 2× SDS sample buffer (Bio-Rad). N2a cells were first collected in Lysis Buffer as described previously. Samples were subject to SDS-PAGE, transferred to nitrocellulose membranes using wet or semi-dry apparati (Mini Trans-Blot Cell or Trans-Blot Turbo Blotting System, respectively, BioRad), and probed with primary antibody (Table S1) in 5% BSA/PBS + 0.1% Tween 20, followed by DyLight 680 or 800 anti-rabbit, anti-mouse (Thermo Scientific) or by HRP conjugated secondaries (Bio-Rad). Membranes were imaged using an Odyssey Infrared Imager (model 9120, LI-COR Biosciences) and protein intensity was measured using the Image Studio Lite software (LI-COR Biosciences).

Fold change calculation

In cycloheximide-chase experiments, the amount of protein remaining after 24h of cycloheximide treatment was calculated as a fraction of the amount of protein in the DMSO treated condition, as previously described [30]. Both levels were previously normalized to the tubulin loading control. The fractional degradative amount of each condition was then normalized to the experimental control by dividing the perturbation condition by the control condition.

Subcellular fractionation with sucrose step gradient

For each gradient, two T75 culture flaks of primary cortical neurons (7,500,000 cells each) were used. All procedures were carried out at 4ºC post-collection and performed as described previously [52], with slight modifications. Briefly, neurons were detached from the flask with TrypLE Express (Life Technologies), and washed once with ice-cold Neurobasal and twice with ice-cold PBS. Neurons were then subject to hypotonic shock and allowed to swell on ice for 15 minutes. After cell resuspension in isotonic conditions, neurons were gently lysed with 3x freeze-thaw cycles. The lysates were centrifuged (2,000 x g, 10 min, 4ºC), and the post-nuclear supernatant (PNS) was brought to 40.6% sucrose and loaded in the bottom of a centrifugation tube, overlaid with 35% sucrose, followed by 25% sucrose and then 8% sucrose solution (in ddH2O, 3 mM imidazole, pH 7.4 with protease and phosphatase inhibitors). After centrifugation in a Beckman centrifuge (3h, 210,000xg, 4ºC), thirteen 100µL fractions were collected and equal volumes were used for Western blotting, as previously described. Relative protein distribution was calculated after determining the optical density of each fraction and further normalizing against the sum of all fractions. Fractions were divided in different groups according to their respective sucrose gradient.

Real-time RT-PCR

RNA was extracted from either cortical neurons or N2a cells using TRIzol (Thermo Fischer), and purified using the Direct-zol RNA MiniPrep Plus kit (Zymo Research). RT-PCR was performed in a StepOnePlus RealTime PCR instrument, with iTaq™ Universal Probes One-Step Kit (Biorad), using pre-designed TaqMan probes. Amplification conditions were the following: initial denaturing at 95ºC for 10 minutes, 40 cycles of denaturarion at 95ºC for 15 seconds and extension at 60ºC for 1 minutes. Rab35 levels were normalized to either β-actin (actb) or TATA-binding protein (tbp). Results presented are normalized to β-actin.

Flow cytometry

N2a cells were detached using TrypLE Express (Life Technologies), for 5 min at 37ºC. After washing, cells were resuspended in ice-cold Flow Buffer (0,2% FBS, 0.5mM EDTA in PBS) and strained through a 35µm nylon mesh to promote single cell suspensions and kept on ice. Cells were analyzed in a BD Fortessa (BD Biosciences). Unstained cells were used as a control for background fluorescence. Flow Cytometry data was analyzed using FCS Express 6 (DeNovo Software).

Ubiquitylation assay

N2a cells were transfected with vectors encoding GFP-Tau and HA-Ubiquitin with either mCherry or mCh-Rab35. After 48h, cells were treated with DMSO vehicle or Dexamethasone, and incubated for another 43h. Cells were then incubated with chloroquine, leupeptin and epoxomicin for 5h. Cell lysates were collected, washed 3x with cold PBS in Lysis buffer (50 mm Tris-Base, 150 mm NaCl, 1% Triton X-100, 0.5% deoxycholic acid) with protease inhibitor (Roche) and phosphatase inhibitor cocktails II and III (Sigma), and clarified by centrifugation at high speed (10 min, 20,000 rcf). Subsequent steps were performed as described in the coimmunoprecipitation section.

Animals and AAV injection

8-10 month old male Wistar Rats (Charles River Laboratories, Spain; N=5 per group) were paired under standard laboratory conditions (8:00 A.M. to 8:00 P.M.; 22 °C) with ad libitum access to food and drink. Animals received daily subcutaneous injections of the synthetic glucocorticoid, dexamethasone (GC) (300 µg/kg; Sigma D1756; dissolved in sesame oil containing 0.01 % ethanol; Sigma S3547) for 14 sequential days, while the other half received daily injections of the vehicle solution (sesame oil with 0.01% ethanol). All experimental procedures were approved by the local

ethical committee of University of Minho and national authority for animal experimentation; all experiments were in accordance with the guidelines for the care and handling of laboratory animals, as described in the Directive 2010/63/EU. For AAV injection experiment (N=6-8 per group), animals were anaesthetised with 75 mg kg−1 ketamine (Imalgene, Merial) plus 0.5 mg kg−1 medetomidine (Dorbene, Cymedica). Virus was bilaterally injected into the dorsal and ventral hippocampus (coordinates from bregma, according to Paxinos and Watson50: -3.0 mm anteroposterior (AP), +-1.6 mm mediolateral (ML), and -3.3 mm dorsoventral (DV) and -6.2 mm AP, +-4.5 mm ML, and -6.0 mm DV, respectively). A total of 2uL was injected at a rate of 200 nL/minute, and the needle was kept in place for 7 minutes before retraction. Rats were removed from the stereotaxic frame, sutured and allowed to recover for three weeks prior to vehicle or dexamethasone treatment.

Subcellular fractionation

To obtain the synaptossome membrane fraction, a previously described fractionation protocol was used [35]. Briefly, hippocampal tissue was homogenized [10× homogenization buffer (sucrose 9%; 5 mM DTT; 2 mM EDTA; 25 mM Tris, pH 7.4); Complete Protease Inhibitor (Roche), and Phosphatase Inhibitor Mixtures II and III (Sigma)] and centrifuged (1,000 × g). The postnuclear supernatant was subsequently centrifuged (12,500 × g) to yield crude synaptosomal and synaptosome-depleted fractions. The latter was ultracentrifuged (176,000 × g) to yield a light membrane/Golgi fraction (P3) and a cytoplasmic fraction (S3). The crude synaptosomal fraction was lysed in a hypo-osmotic solution and then centrifuged (25,000 × g) to obtain the synaptosomal fraction (LP1).

Neurostructural analysis

As previously described, half of each rat brain (N=6–7 per group) was immersed in Golgi-Cox solution for 7-10 days. After transfer to tissue protectant solution, vibratome-cut coronal brain sections (200

μm thick) were used. After development, fixation and dehydration, slides were used to perform three-dimensional morphometric analysis. Dendritic arborization and spines were analyzed in dorsal hippocampus (CA1 area). All neuronal dendritic trees were reconstructed at ×600 (oil) magnification using a motorized microscope (Axioplan2, Zeiss) and Neurolucida software (MBF Bioscience). For spine analysis, proximal and distal apical dendritic segments (30 μm) were randomly selected and spines were counted and further classified in immature (thin) and complex/mature (mushroom, wide/thick, and ramified) categories as previously described [13]. 3 different dendritic segments were selected per neuron.

Rab35 glucocorticoid receptor (GR) binding

Binding sites were analyzed with the use of the GTRD database (http://gtrd.biouml.org/)[53], which is the largest aggregation of ChIP-seq experiment raw data for the human and mouse genome from publically available sources (including GEO, SRA, Encode) using a unified alignment and ChIP-seq peak calling. Peaks were merged into clusters and unique metaclusters (approx. 70M to ensure that transcription factor binding sites are not non-redundant. Our analysis focused on the mouse *Rab35* gene since there is no such comprehensive Chip-seq database for other rodents species. In the search for GR binding sites, we permitted a maximum distance of 1000 nucleotides from *Rab35*.

Statistical Analysis

Graphing and statistics analysis were performed using Prism (GraphPad). Shapiro-Wilk normality test was used to determine if data sets were modeled by a normal distribution. Unpaired, two-tailed t tests, one-way ANOVA or two-way ANOVAs were used with values of $p<0.05$ being considered as significantly different.

References

1 Roberson, E. D. *et al.* Reducing endogenous tau ameliorates amyloid beta-induced deficits in an Alzheimer's disease mouse model. *Science* **316**, 750-754, doi:10.1126/science.1141736 (2007).

2 Ittner, L. M. *et al.* Dendritic function of tau mediates amyloid-beta toxicity in Alzheimer's disease mouse models. *Cell* **142**, 387-397, doi:10.1016/j.cell.2010.06.036 (2010).

3 Guo, T., Noble, W. & Hanger, D. P. Roles of tau protein in health and disease. *Acta Neuropathol* **133**, 665-704, doi:10.1007/s00401-017-1707-9 (2017).

4 Kimura, T. *et al.* Hyperphosphorylated tau in parahippocampal cortex impairs place learning in aged mice expressing wild-type human tau. *EMBO J* **26**, 5143-5152, doi:10.1038/sj.emboj.7601917 (2007).

5 Yin, Y. *et al.* Tau accumulation induces synaptic impairment and memory deficit by calcineurin-mediated inactivation of nuclear CaMKIV/CREB signaling. *Proc Natl Acad Sci U S A* **113**, E3773-3781, doi:10.1073/pnas.1604519113 (2016).

6 Vossel, K. A. *et al.* Tau reduction prevents Abeta-induced defects in axonal transport. *Science* **330**, 198, doi:10.1126/science.1194653 (2010).

7 Zempel, H., Thies, E., Mandelkow, E. & Mandelkow, E. M. Abeta oligomers cause localized Ca(2+) elevation, missorting of endogenous Tau into dendrites, Tau phosphorylation, and destruction of microtubules and spines. *J Neurosci* **30**, 11938-11950, doi:10.1523/JNEUROSCI.2357-10.2010 (2010).

8 Sotiropoulos, I. *et al.* Atypical, non-standard functions of the microtubule associated Tau protein. *Acta Neuropathol Commun* **5**, 91, doi:10.1186/s40478-017-0489-6 (2017).

9 Vyas, S. *et al.* Chronic Stress and Glucocorticoids: From Neuronal Plasticity to Neurodegeneration. *Neural plasticity* **2016**, 6391686, doi:10.1155/2016/6391686 (2016).

10 Lopes, S. *et al.* Absence of Tau triggers age-dependent sciatic nerve morphofunctional deficits and motor impairment. *Aging cell* **15**, 208-216, doi:10.1111/acel.12391 (2016).

11 Lopes, S. *et al.* Tau Deletion Prevents Stress-Induced Dendritic Atrophy in Prefrontal Cortex: Role of Synaptic Mitochondria. *Cereb Cortex*, doi:10.1093/cercor/bhw057 (2016).

12 Pallas-Bazarra, N. *et al.* Novel function of Tau in regulating the effects of external stimuli on adult hippocampal neurogenesis. *EMBO J* **35**, 1417-1436, doi:10.15252/embj.201593518 (2016).

13 Pinheiro, S. *et al.* Tau Mislocation in Glucocorticoid-Triggered Hippocampal Pathology. *Mol Neurobiol*, doi:10.1007/s12035-015-9356-2 (2015).

14 Dioli, C. *et al.* Tau-dependent suppression of adult neurogenesis in the stressed hippocampus. *Mol Psychiatry* **22**, 1110-1118, doi:10.1038/mp.2017.103 (2017).

15 Khanna, M. R., Kovalevich, J., Lee, V. M., Trojanowski, J. Q. & Brunden, K. R. Therapeutic strategies for the treatment of tauopathies: Hopes and challenges. *Alzheimer's & dementia : the journal of the Alzheimer's Association* **12**, 1051-1065, doi:10.1016/j.jalz.2016.06.006 (2016).

16 Lee, M. J., Lee, J. H. & Rubinsztein, D. C. Tau degradation: the ubiquitin-proteasome system versus the autophagy-lysosome system. *Prog Neurobiol* **105**, 49-59, doi:10.1016/j.pneurobio.2013.03.001 (2013).

17 Zhang, Y., Chen, X., Zhao, Y., Ponnusamy, M. & Liu, Y. The role of ubiquitin proteasomal system and autophagy-lysosome pathway in Alzheimer's disease. *Rev Neurosci*, doi:10.1515/revneuro-2017-0013 (2017).

18 Zhang, J. Y., Liu, S. J., Li, H. L. & Wang, J. Z. Microtubule-associated protein tau is a substrate of ATP/Mg(2+)-dependent proteasome protease system. *J Neural Transm (Vienna)* **112**, 547-555, doi:10.1007/s00702-004-0196-x (2005).

19 Hamano, T. *et al.* Autophagic-lysosomal perturbation enhances tau aggregation in transfectants with induced wild-type tau expression. *Eur J Neurosci* **27**, 1119-1130, doi:10.1111/j.1460-9568.2008.06084.x (2008).
20 Small, S. A. S.-S., S.; Mayeux, R.; Petsko, G.A. Endosomal traffick jams represent a pathogenic hub and therapeutic target in Alzheimer's disease. *Trends in Neurosciences* **40**, 592-602 (2017).
21 Kett, L. R. & Dauer, W. T. Endolysosomal dysfunction in Parkinson's disease: Recent developments and future challenges. *Mov Disord* **31**, 1433-1443, doi:10.1002/mds.26797 (2016).
22 Rivero-Rios, P. *et al.* Alterations in late endocytic trafficking related to the pathobiology of LRRK2-linked Parkinson's disease. *Biochem Soc Trans* **43**, 390-395, doi:10.1042/BST20140301 (2015).
23 Georgieva, E. R., Xiao, S., Borbat, P. P., Freed, J. H. & Eliezer, D. Tau binds to lipid membrane surfaces via short amphipathic helices located in its microtubule-binding repeats. *Biophys J* **107**, 1441-1452, doi:10.1016/j.bpj.2014.07.046 (2014).
24 Pooler, A. M. & Hanger, D. P. Functional implications of the association of tau with the plasma membrane. *Biochem Soc Trans* **38**, 1012-1015, doi:10.1042/BST0381012 (2010).
25 Raiborg, C. & Stenmark, H. The ESCRT machinery in endosomal sorting of ubiquitylated membrane proteins. *Nature* **458**, 445-452, doi:10.1038/nature07961 (2009).
26 Frankel, E. B. & Audhya, A. ESCRT-dependent cargo sorting at multivesicular endosomes. *Semin Cell Dev Biol*, doi:10.1016/j.semcdb.2017.08.020 (2017).
27 Hoover, B. R. *et al.* Tau mislocalization to dendritic spines mediates synaptic dysfunction independently of neurodegeneration. *Neuron* **68**, 1067-1081, doi:10.1016/j.neuron.2010.11.030 (2010).
28 Maminska, A. *et al.* ESCRT proteins restrict constitutive NF-kappaB signaling by trafficking cytokine receptors. *Sci Signal* **9**, ra8, doi:10.1126/scisignal.aad0848 (2016).
29 Edgar, J. R., Willen, K., Gouras, G. K. & Futter, C. E. ESCRTs regulate amyloid precursor protein sorting in multivesicular bodies and intracellular amyloid-beta accumulation. *J Cell Sci* **128**, 2520-2528, doi:10.1242/jcs.170233 (2015).
30 Sheehan, P., Zhu, M., Beskow, A., Vollmer, C. & Waites, C. L. Activity-Dependent Degradation of Synaptic Vesicle Proteins Requires Rab35 and the ESCRT Pathway. *J Neurosci* **36**, 8668-8686, doi:10.1523/JNEUROSCI.0725-16.2016 (2016).
31 Subach, F. V. *et al.* Monomeric fluorescent timers that change color from blue to red report on cellular trafficking. *Nat Chem Biol* **5**, 118-126, doi:10.1038/nchembio.138 (2009).
32 Fernandes, A. C. *et al.* Reduced synaptic vesicle protein degradation at lysosomes curbs TBC1D24/sky-induced neurodegeneration. *J Cell Biol* **207**, 453-462, doi:10.1083/jcb.201406026 (2014).
33 Johansson, L. *et al.* Midlife psychological stress and risk of dementia: a 35-year longitudinal population study. *Brain* **133**, 2217-2224, doi:10.1093/brain/awq116 (2010).
34 Machado, A. *et al.* Chronic stress as a risk factor for Alzheimer's disease. *Rev Neurosci* **25**, 785-804, doi:10.1515/revneuro-2014-0035 (2014).
35 Lopes, S. *et al.* Tau protein is essential for stress-induced brain pathology. *Proc Natl Acad Sci U S A* **113**, E3755-3763, doi:10.1073/pnas.1600953113 (2016).
36 Green, K. N., Billings, L. M., Roozendaal, B., McGaugh, J. L. & LaFerla, F. M. Glucocorticoids increase amyloid-beta and tau pathology in a mouse model of Alzheimer's disease. *J Neurosci* **26**, 9047-9056, doi:10.1523/JNEUROSCI.2797-06.2006 (2006).
37 Sotiropoulos, I. *et al.* Stress acts cumulatively to precipitate Alzheimer's disease-like tau pathology and cognitive deficits. *J Neurosci* **31**, 7840-7847, doi:10.1523/JNEUROSCI.0730-11.2011 (2011).

38 Chesser, A. S., Pritchard, S. M. & Johnson, G. V. Tau clearance mechanisms and their possible role in the pathogenesis of Alzheimer disease. *Front Neurol* **4**, 122, doi:10.3389/fneur.2013.00122 (2013).
39 Caballero, B. *et al.* Interplay of pathogenic forms of human tau with different autophagic pathways. *Aging cell*, doi:10.1111/acel.12692 (2017).
40 Sahu, R. *et al.* Microautophagy of cytosolic proteins by late endosomes. *Dev Cell* **20**, 131-139, doi:10.1016/j.devcel.2010.12.003 (2011).
41 Oshima, R. *et al.* ESCRT-0 dysfunction compromises autophagic degradation of protein aggregates and facilitates ER stress-mediated neurodegeneration via apoptotic and necroptotic pathways. *Scientific reports* **6**, 24997, doi:10.1038/srep24997 (2016).
42 Watson, J. A. *et al.* Motor and Sensory Deficits in the teetering Mice Result from Mutation of the ESCRT Component HGS. *PLoS Genet* **11**, e1005290, doi:10.1371/journal.pgen.1005290 (2015).
43 Clayton, E. L. *et al.* Frontotemporal dementia caused by CHMP2B mutation is characterised by neuronal lysosomal storage pathology. *Acta Neuropathol* **130**, 511-523, doi:10.1007/s00401-015-1475-3 (2015).
44 Zhang, Y. *et al.* Patient iPSC-Derived Neurons for Disease Modeling of Frontotemporal Dementia with Mutation in CHMP2B. *Stem cell reports* **8**, 648-658, doi:10.1016/j.stemcr.2017.01.012 (2017).
45 Nixon, R. A. & Yang, D. S. Autophagy failure in Alzheimer's disease--locating the primary defect. *Neurobiol Dis* **43**, 38-45, doi:10.1016/j.nbd.2011.01.021 (2011).
46 Suzuki, K. *et al.* Neurofibrillary tangles in Niemann-Pick disease type C. *Acta Neuropathol* **89**, 227-238 (1995).
47 Ross, J. A., Gliebus, G. & Van Bockstaele, E. J. Stress induced neural reorganization: A conceptual framework linking depression and Alzheimer's disease. *Prog Neuropsychopharmacol Biol Psychiatry*, doi:10.1016/j.pnpbp.2017.08.004 (2017).
48 Sotiropoulos, I. *et al.* Stress and glucocorticoid footprints in the brain-the path from depression to Alzheimer's disease. *Neurosci Biobehav Rev* **32**, 1161-1173, doi:10.1016/j.neubiorev.2008.05.007 (2008).
49 Sotiropoulos, I. *et al.* Glucocorticoids trigger Alzheimer disease-like pathobiochemistry in rat neuronal cells expressing human tau. *J Neurochem* **107**, 385-397, doi:10.1111/j.1471-4159.2008.05613.x (2008).
50 Kontaxi, C., Piccardo, P. & Gill, A. C. Lysine-Directed Post-translational Modifications of Tau Protein in Alzheimer's Disease and Related Tauopathies. *Front Mol Biosci* **4**, 56, doi:10.3389/fmolb.2017.00056 (2017).
51 Sousa, N. & Almeida, O. F. Disconnection and reconnection: the morphological basis of (mal)adaptation to stress. *Trends Neurosci* **35**, 742-751, doi:10.1016/j.tins.2012.08.006 (2012).
52 de Araujo, M. E., Huber, L. A. & Stasyk, T. Isolation of endocitic organelles by density gradient centrifugation. *Methods Mol Biol* **424**, 317-331, doi:10.1007/978-1-60327-064-9_25 (2008).
53 Yevshin, I., Sharipov, R., Valeev, T., Kel, A. & Kolpakov, F. GTRD: a database of transcription factor binding sites identified by ChIP-seq experiments. *Nucleic Acids Res* **45**, D61-D67, doi:10.1093/nar/gkw951 (2017).

Figure Legends

Figure 1. Tau protein localizes to early endosomes and MVBs. (A) Electron micrographs of immunogold-labeled Tau (arrows) in multivesicular bodies (yellow dashed lines) of rat hippocampus (scale bar: 250nm). (B) Schematic diagram of proximity ligation assay (PLA), wherein primary antibodies against Hrs or Tau are detected by secondary antibodies conjugated to DNA. Ligation and amplification of DNA, resulting in green signal, only occurs when proteins are in close (20-50 nm) proximity. (C) PLA signal (green) for Hrs/Tau interaction (arrows) on an mCh-Hrs-labeled endosome (red) in N2a cells; scale bar: 5 μm (see also Fig. S1). (D) Super-resolution images of N2a cells transfected with mCh-Hrs and immunostained for Tau and EEA1. Higher-magnification insets (A and B) show Hrs- and EEA1-positive endosomes with juxtaposed Tau puncta present both in the membrane and lumen; scale bar: 5 μm. (E) Super-resolution images of N2a cells transfected with constitutively-active Rab5 (EGFP-Rab5-CA) and immunostained for Tau, again revealing the presence of Tau in both membranes and lumen of early endosomes (scale bar: 10 μm).

Figure 2. Tau degradation occurs through the Rab35/ESCRT pathway. (A) Schematic diagram of the Rab35/ESCRT pathway indicating our manipulations to increase (overexpression; green) or decrease (knockdown; red) its activity. (B-C) Representative immunoblots (B) and quantification of Tau degradation (C) from 14 DIV primary neurons transduced with EGFP or shTSG101, treated for 24 h with either DMSO (CON) or cycloheximide (CHX), and probed for Tau, TSG101, and tubulin. shTSG101-expressing neurons exhibit markedly decreased Tau degradation compared to EGFP-expressing controls (n=18-19 per condition). (D) shTSG101 significantly decreases TSG101 protein levels (n=12-14/condition). (E-F) Representative immunoblots (E) and quantification of Tau degradation (F) from 14 DIV neurons transduced with mCh or mCh-TSG101, treated for 24 h with either DMSO (CON) or cycloheximide (CHX), and probed for Tau and tubulin. Overexpression of TSG101 increases Tau degradation (n=17/condition). (G-H) Representative immunoblots (G) and

quantification of Tau degradation (H) from 14 DIV neurons transduced EGFP or shRab35, treated for 24 h with either DMSO (CON) or cycloheximide (CHX), and probed for Tau, Rab35, and tubulin. shRab35-expressing neurons exhibit markedly decreased Tau degradation compared to EGFP-expressing controls (n=23-26 per condition). (I) shRab35 significantly decreases Rab35 protein levels (n=4/condition). (J-K) Representative immunoblots (J) and quantification of Tau degradation (K) from 14 DIV neurons transduced with mCh or mCh-Rab35, treated for 24 h with either DMSO (CON) or cycloheximide (CHX), and probed for Tau or tubulin. Rab35 overexpression increases Tau degradation (n=18 per condition). (L) Flow cytometry distribution of N2a cells cotransfected with either HA vector (black) or HA-Rab35 (green) and medium FT-tagged wild-type Tau (FT-Tau); blue fluorescence (y axis) indicates "younger" Tau protein while red fluorescence (x axis) indicates "older" Tau. (M) The ratio of cells expressing red to blue (older:younger) FT-wtTau is reduced in cells overexpressing Rab35, indicating faster Tau turnover (n=9/condition). (N) The ratio of cells expressing red to blue FT-tagged phospho-mimetic E14 Tau is also reduced in cells overexpressing Rab35, indicating faster turnover of 'hyperphosphorylated' Tau (n=10/condition). All numeric data represent mean ± SEM (unpaired student's t-test; *p<0.05; **p<0.01; ***p<0.001; ****p<0.0001).

Figure 3: Rab35 regulates degradation of PHF1 and Ser262 phospho-Tau through the ESCRT pathway. (A-B) Representative immunoblots (A) and quantification of Tau degradation (B) from 14 DIV primary neurons transduced with EGFP or shRab35, treated for 24 h with either DMSO (CON) or cycloheximide (CHX), and probed for PHF1, Ser262, or CP13 Tau and tubulin. shRab35-expressing neurons exhibit markedly decreased Ser262 and PHF1 Tau degradation compared to EGFP-expressing controls, while CP13 degradation is unaffected (n=4 per condition for PHF1 and CP13, n=3 for Ser262). (C) Images of PLA signal (green) for Hrs/Tau interaction in N2a cells co-transfected with FLAG-Hrs and either mCh or mCh-Rab35 (red), and probed with antibodies against FLAG and total (DA9) or phospho-Tau species (PHF1, Ser262, or CP13); scale bar: 10 μm. (D) Rab35 overexpression

significantly increases PLA puncta for total, PHF1, and Ser262 Tau, but not CP13 (n=121-132 cells for total Tau, 178-195 cells for PHF1, 71-98 cells for Ser262, 25-29 cells for CP13; Mann-Whitney test). Unless otherwise indicated, numeric data represent mean ± SEM (unpaired student's t-test; *p<0.05; ** p<0.01; ****p<0.0001).

Figure 4: Rab35/ESCRT pathway promotes Tau sorting to lysosomes and targets both axonal and somatodendritic Tau pools.

(A-B) Representative images and quantification of 14 DIV neurons transduced with mCh, mCh-TSG101, or mCh-Rab35, treated for 5 h with either DMSO (CON) or Bafilomycin (Baf) to block lysosomal degradation, and immunostained for Tau and LAMP1. Overexpression of Rab35 or TSG101 increases Tau accumulation in lysosomes of Baf-treated neurons, indicating that Rab35/ESCRT pathway activation stimulates sorting of Tau into lysosomes (scale bar: 5 µm)(n=25-27 cells/condition; for TSG101, 2-way ANOVA, *Baf* x *TSG101* interaction $F_{1, 101}$=4,328 p=0.04, overall *Baf* effect $F_{1, 101}$=10,68 p=0.0015, Sidak posthoc analysis ** p<0.01; for Rab35, 2-way ANOVA, *Baf* x *Ra35* interaction $F_{1, 101}$=5,36 p=0.02, overall *Baf* effect $F_{1, 101}$=12,01 p=0.0008, Sidak posthoc analysis *** p<0.001). All numeric data represent mean ± SEM. (C) Images of 14 DIV neurons transduced with mCh or mCh-Rab35, treated for 24 h with either DMSO (CON) or cycloheximide (CHX) and immunostained for Tau; scale bar: 10 µm. (D) Tau fluorescence intensity is markedly reduced in both soma and axons of CHX-treated neurons overexpressing Rab35 compared to mCh, indicating faster Tau degradation (n=24/condition; for axons, n=25-26/condition); for soma, 2-way ANOVA, overall *CHX* effect $F_{1, 92}$=19.27 p<0.0001, Sidak posthoc analysis *** p<0.001; for axon, 2-way ANOVA, *CHX* x *Rab35* interaction $F_{1, 97}$=13.27 p=0.0004, overall *CHX* effect $F_{1, 97}$=14.34, p=0.0003, Sidak posthoc analysis **** p<0.0001).

Figure 5. Glucocorticoids decrease Rab35 levels *in vitro* and *in vivo*. (A-B) Representative immunoblots (A) and quantification of Hrs, TSG101, CHMP2b, and Rab35 protein levels (B) from 14 DIV neurons treated with either DMSO (CON) or glucocorticoids (GC). GC treatment selectively decreases Rab35 without affecting levels of Hrs, TSG101, or CHMP2b (n=9-10/condition). (C) Rab35 mRNA levels are decreased by GC in 14 DIV hippocampal neurons and N2a cells (for neurons, n=9/condition; for N2a cells, n=6/condition). (D) Schematic diagram of GC and vehicle control (CON) treatment in rats for 15 days. (E-F) Representative immunoblots (E) and quantification of Rab protein levels (F) in hippocampus of GC and CON animals. Levels of Rab35, but not other Rabs, are decreased in GC vs. CON animals (n=5 animals/condition). (G) Immunofluorescence staining of Rab35 (green) and DAPI (blue) in hippocampus of GC and CON animals. (H) Quantification of the Rab35 integrated fluorescent density in CA1 area in CON and GC groups (n=5 animals, 3 slices per animal; ** $p<0.01$; Mann-Whitney Test). All numeric data represent mean ± SEM (unpaired student's t-test *$p<0.05$; ** $p<0.01$).

Figure 6. Rab35 overexpression rescues glucocorticoid-induced Tau accumulation and associated neuronal atrophy. (A-B) Representative immunoblots (A) and quantification of Tau degradation (B) in 14 DIV neurons expressing mCh-Rab35 or mCh, treated for 24 h with cycloheximide (CHX) or DMSO (CON) under GC conditions. GC significantly decreases Tau degradation, whereas Rab35 overexpression blocks this effect (n=12-14/condition; * $p<0.05$; 1-way ANOVA, Dunnet post-hoc analysis). (C) Injection of AAV to express EGFP or EGFP-Rab35, driven by the CaMKII promoter, in hippocampus of rats prior to GC or vehicle control (CON) treatment. **(**D) Representative immunoblots (D) and quantification of Tau levels (E) in hippocampal synaptosomes reveal that GC increases total Tau levels in animals expressing EGFP, but not Rab35 (n=6 animals/group, 2 replicates, 2-way ANOVA, *GC* x *Rab35* interaction $F_{1, 39}=10,51$ $p=0.002$; Sidak posthoc analysis *$p<0.05$). (F) Golgi-based 3D neuronal reconstruction of hippocampal pyramidal

neurons (CA1 area). (G) GC treatment reduces the length of apical dendrites in animals expressing EGFP, but not Rab35 (n=6-7 animals/group; 6-8 neurons/animal, 2-way ANOVA , *GC* x *Rab35* interaction $F_{1, 155}$=3.969 p=0.0481, overall *GC* effect $F_{1, 155}$=8.998 p=0.0031, Sidak posthoc analysis **p<0.01). (H) Mature spine density is reduced by GC treatment in animals expressing EGFP but not Rab35 (2-way ANOVA, *GC* x *Rab35* interaction $F_{1, 499}$=12.33 p=0.0005, overall *GC* effect $F_{1, 499}$=4.373 p=0.0370, Sidak posthoc analysis * p<0.05; n=6-7 animals/group; 6-8 neurons per animal). (I-J) Sholl analysis of apical dendrites shows reduced dendritic intersections after GC treatment in EGFP- but not Rab35-expressing animals (3-way ANOVA, *GC* x *Rab35* interaction $F_{1, 4212}$= 14,926 p<0.0001, Simple effect analysis, Sidak test for multiple comparisons *p<0.05 **p<0.01 ***p<0.001, n=6-7 animals/group, 6-8 neurons per animal). All numeric data represent mean ± SEM.

Figure 7. GC inhibits Tau degradation via the Rab35/ESCRT pathway.

(A) Working model of Tau degradation through the Rab35/ESCRT pathway, and its inhibition by glucocorticoids. Rab35 mediates Tau clearance via the endo-lysosomal pathway by recruiting initial ESCRT component Hrs, which recognizes and sorts ubiquitylated Tau into early endosomes for packaging into MVBs. This pathway is impaired by high GC levels, as GR activation suppresses transcription of Rab35, which in turn decreases Tau sorting into MVBs and its subsequent degradation by lysosomes.

Table 1. Chromosomal position of GR binding sites for *Rab35* gene. Our analysis identified 14 distinct glucocorticoid response elements associated with the *Rab35* gene, indicating the relevance of glucocorticoids for regulating *Rab35* transcription.

Figure 1

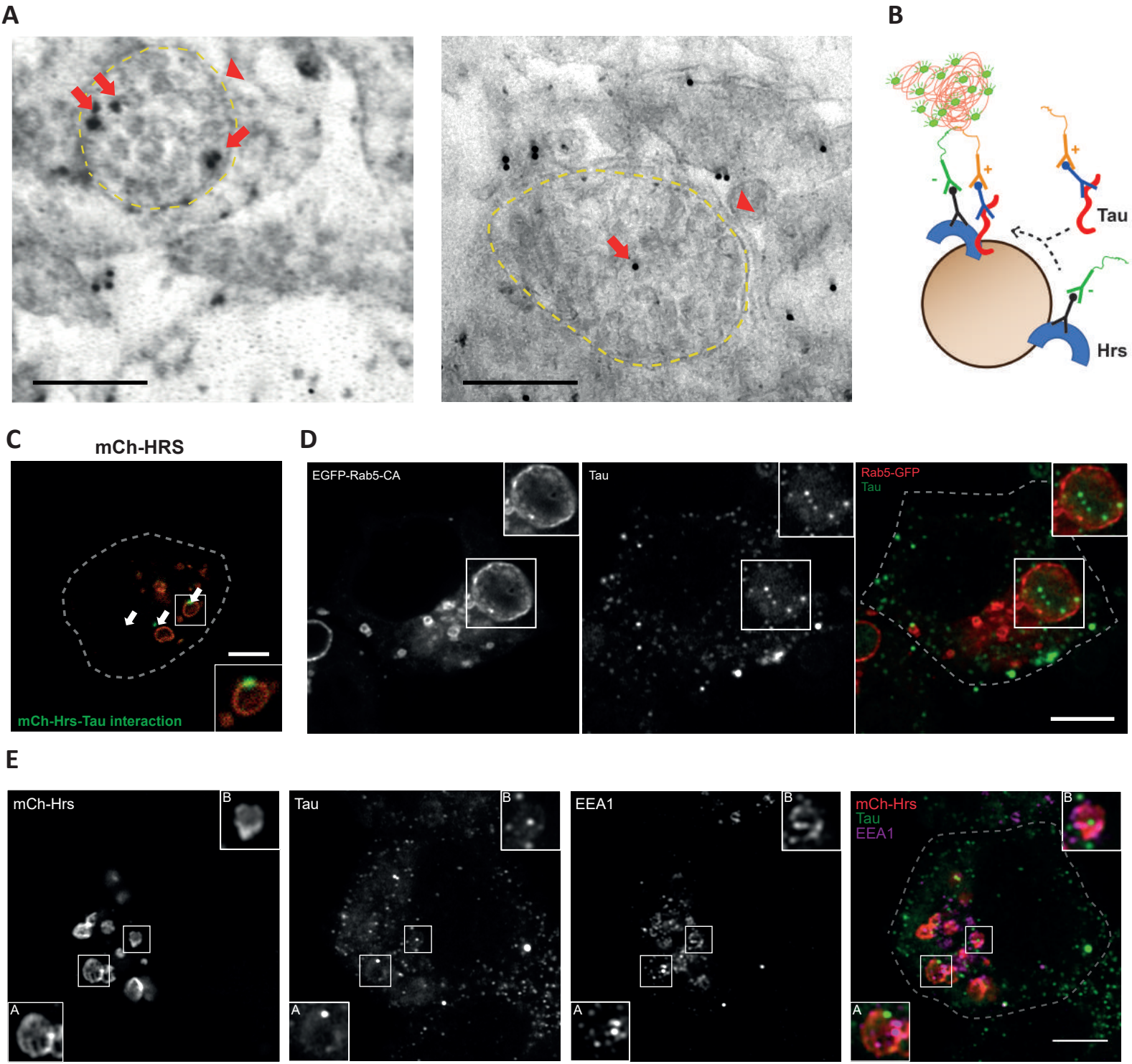
A
B
Tau
Hrs
C
mCh-HRS
mCh-Hrs-Tau interaction
D
EGFP-Rab5-CA
Tau
Rab5-GFP
Tau
E
mCh-Hrs
B
A
Tau
B
A
EEA1
B
A
mCh-Hrs
Tau
EEA1
B
A

Figure 2

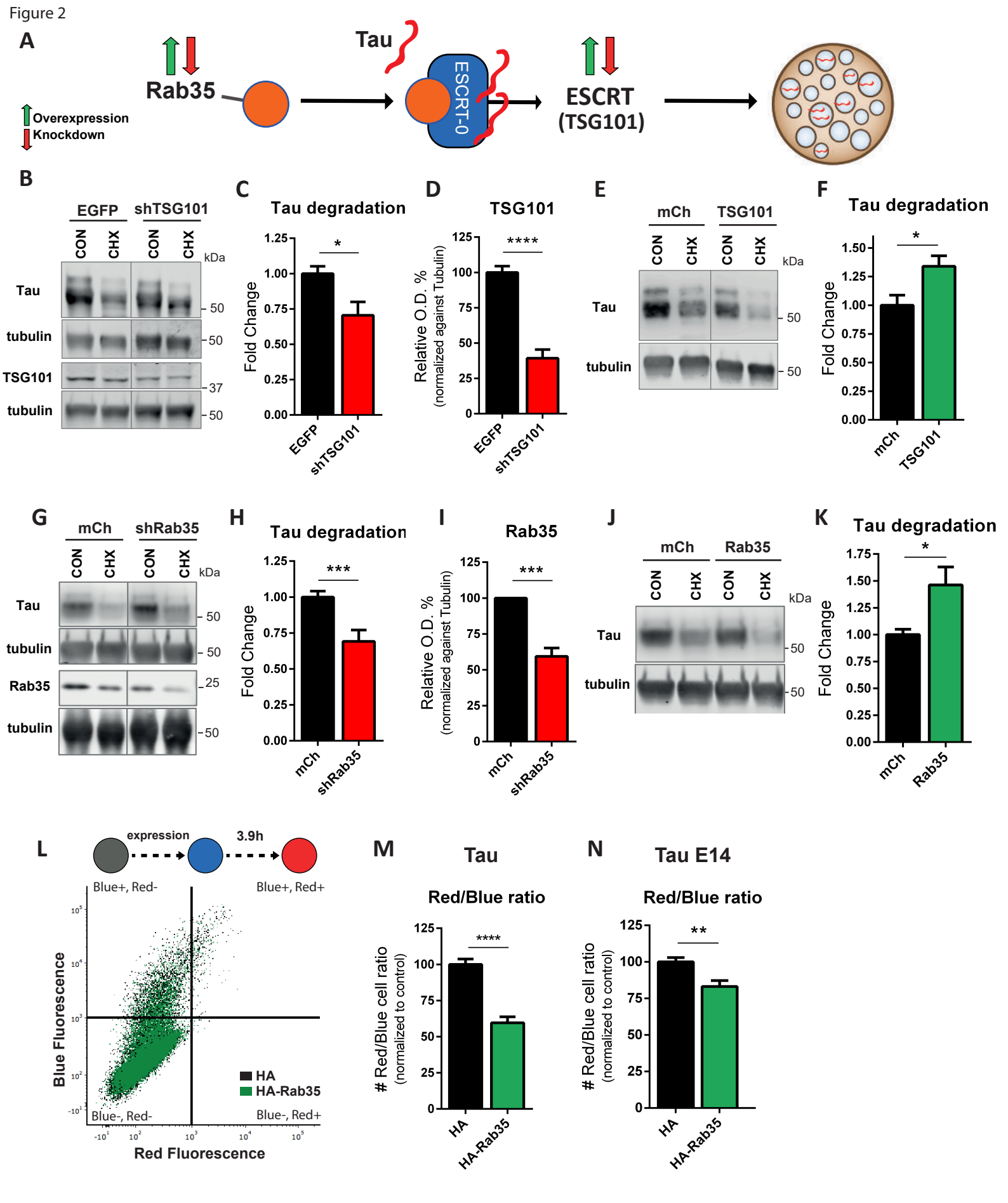
A
Overexpression
Knockdown
Rab35
Tau
ESCRT-0
ESCRT
(TSG101)
B
EGFP
shTSG101
CON
CHX
CON
CHX
kDa
Tau
tubulin
TSG101
tubulin
50
50
37
50
C
Tau degradation
Fold Change
EGFP
shTSG101
D
TSG101
Relative O.D. %
(normalized against Tubulin)
EGFP
shTSG101
E
mCh
TSG101
Tau
tubulin
F
Tau degradation
Fold Change
mCh
TSG101
G
mCh
shRab35
Tau
tubulin
Rab35
tubulin
25
H
Tau degradation
Fold Change
mCh
shRab35
I
Rab35
Relative O.D. %
(normalized against Tubulin)
mCh
shRab35
J
mCh
Rab35
Tau
tubulin
K
Tau degradation
Fold Change
mCh
Rab35
L
expression
3.9h
Blue+, Red-
Blue+, Red+
Blue-, Red-
Blue-, Red+
Blue Fluorescence
Red Fluorescence
HA
HA-Rab35
M
Tau
Red/Blue ratio
Red/Blue cell ratio
(normalized to control)
HA
HA-Rab35
N
Tau E14
Red/Blue ratio
Red/Blue cell ratio
(normalized to control)
HA
HA-Rab35

Figure 3

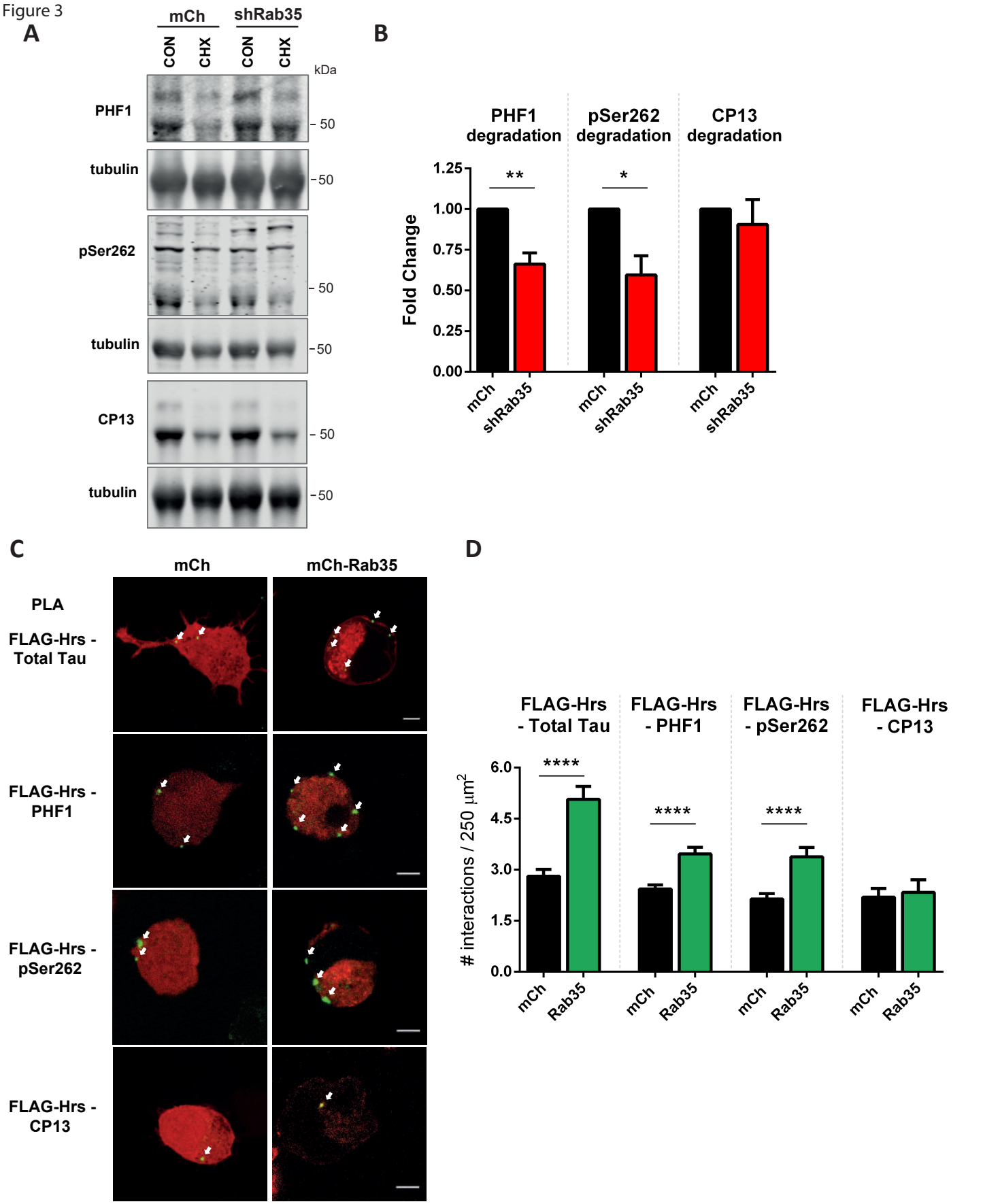
A
mCh
shRab35
CON
CHX
CON
CHX
kDa
PHF1
tubulin
pSer262
tubulin
CP13
tubulin
50
B
PHF1 degradation
pSer262 degradation
CP13 degradation
Fold Change
1.25
1.00
0.75
0.50
0.25
0.00
**
*
mCh
shRab35
C
mCh
mCh-Rab35
PLA
FLAG-Hrs - Total Tau
FLAG-Hrs - PHF1
FLAG-Hrs - pSer262
FLAG-Hrs - CP13
D
FLAG-Hrs - Total Tau
FLAG-Hrs - PHF1
FLAG-Hrs - pSer262
FLAG-Hrs - CP13
interactions / 250 µm2
6.0
4.5
3.0
1.5
0.0
****
mCh
Rab35

Figure 4

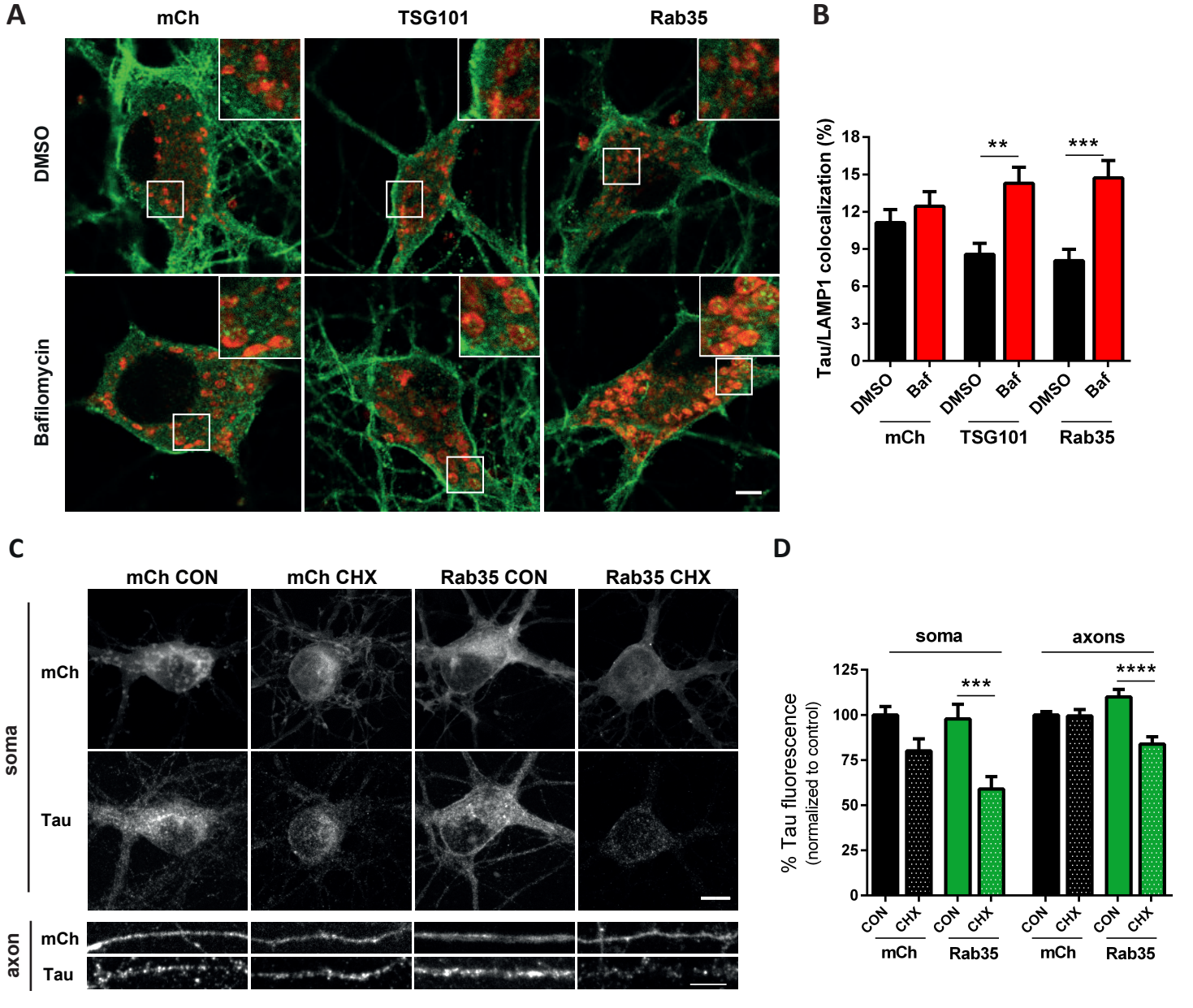
A
mCh
TSG101
Rab35
DMSO
Bafilomycin
B
Tau/LAMP1 colocalization (%)
18
15
12
9
6
3
0
**
***
DMSO
Baf
DMSO
Baf
DMSO
Baf
mCh
TSG101
Rab35
C
mCh CON
mCh CHX
Rab35 CON
Rab35 CHX
soma
mCh
Tau
axon
mCh
Tau
D
soma
axons
% Tau fluorescence
(normalized to control)
125
100
75
50
25
0
***
****
CON
CHX
CON
CHX
CON
CHX
CON
CHX
mCh
Rab35
mCh
Rab35

Figure 5

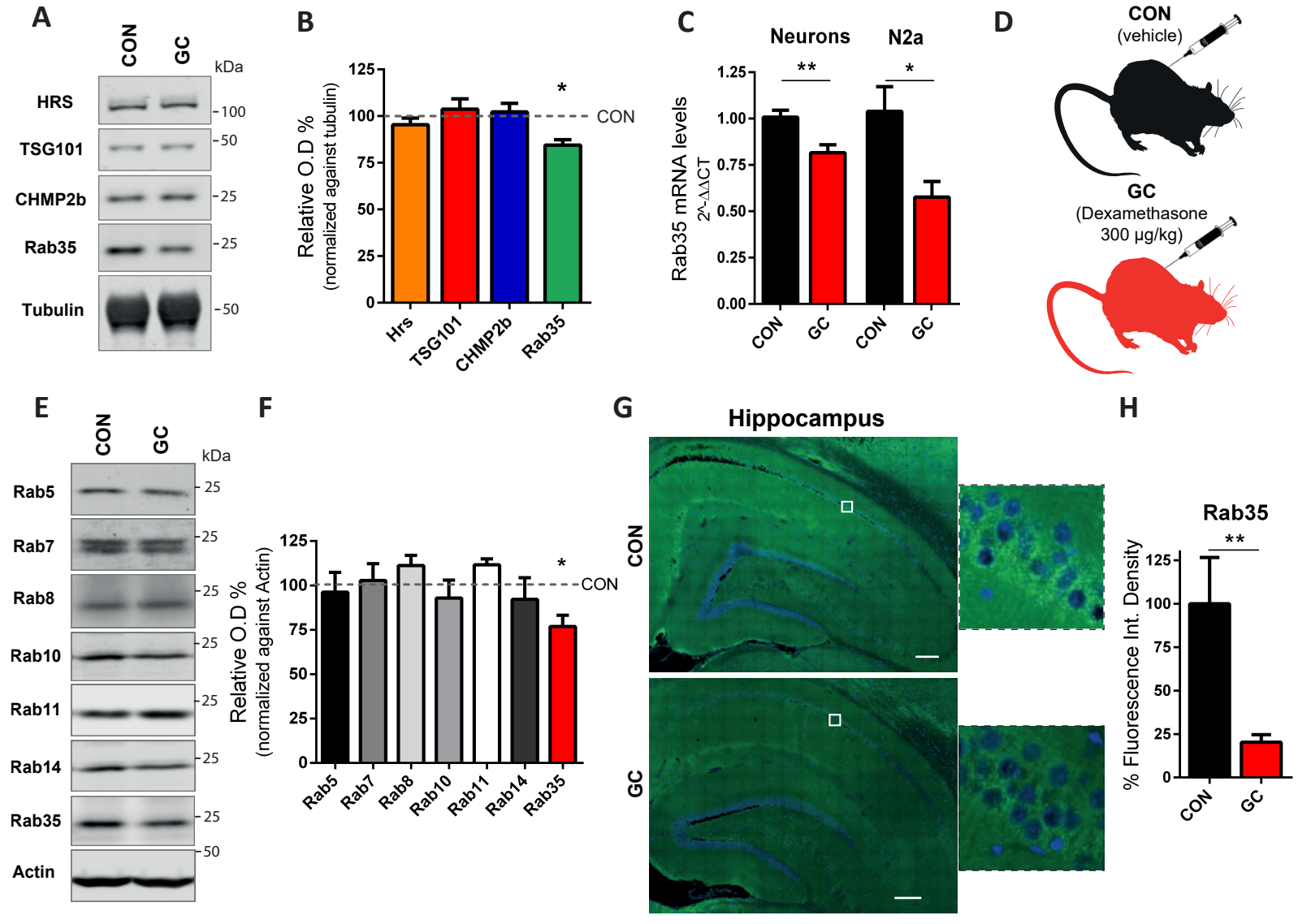
A
CON
GC
kDa
HRS
TSG101
CHMP2b
Rab35
Tubulin
100
50
25
25
50
B
Relative O.D %
(normalized against tubulin)
125
100
75
50
25
0
*
CON
Hrs
TSG101
CHMP2b
Rab35
C
Neurons
N2a
Rab35 mRNA levels
2^-ΔΔCT
1.25
1.00
0.75
0.50
0.25
0.00
**
*
CON
GC
CON
GC
D
CON
(vehicle)
GC
(Dexamethasone
300 µg/kg)
E
CON
GC
kDa
Rab5
Rab7
Rab8
Rab10
Rab11
Rab14
Rab35
Actin
25
25
25
25
25
25
25
50
F
Relative O.D %
(normalized against Actin)
125
100
75
50
25
0
*
CON
Rab5
Rab7
Rab8
Rab10
Rab11
Rab14
Rab35
G
Hippocampus
CON
GC
H
Rab35
**
% Fluorescence Int. Density
125
100
75
50
25
0
CON
GC

Figure 6

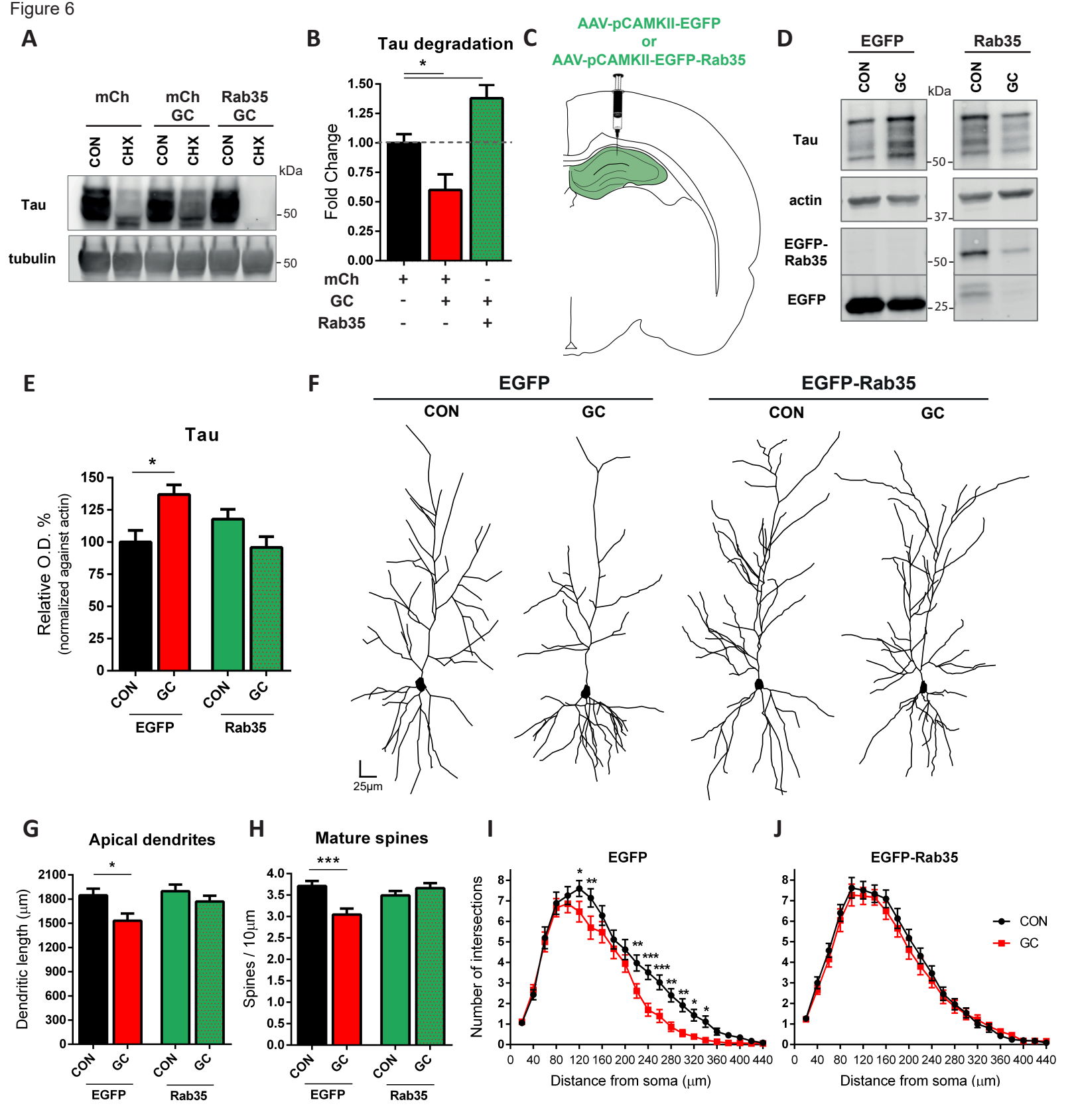
A
mCh
mCh GC
Rab35 GC
CON
CHX
kDa
Tau
tubulin
50
B
Tau degradation
Fold Change
mCh
GC
Rab35
C
AAV-pCAMKII-EGFP
or
AAV-pCAMKII-EGFP-Rab35
D
EGFP
Rab35
actin
EGFP-Rab35
37
25
E
Tau
Relative O.D. %
(normalized against actin)
F
EGFP
EGFP-Rab35
25μm
G
Apical dendrites
Dendritic length (μm)
H
Mature spines
Spines / 10μm
I
EGFP
Number of intersections
Distance from soma (μm)
J
EGFP-Rab35
CON
GC

Figure 7

A

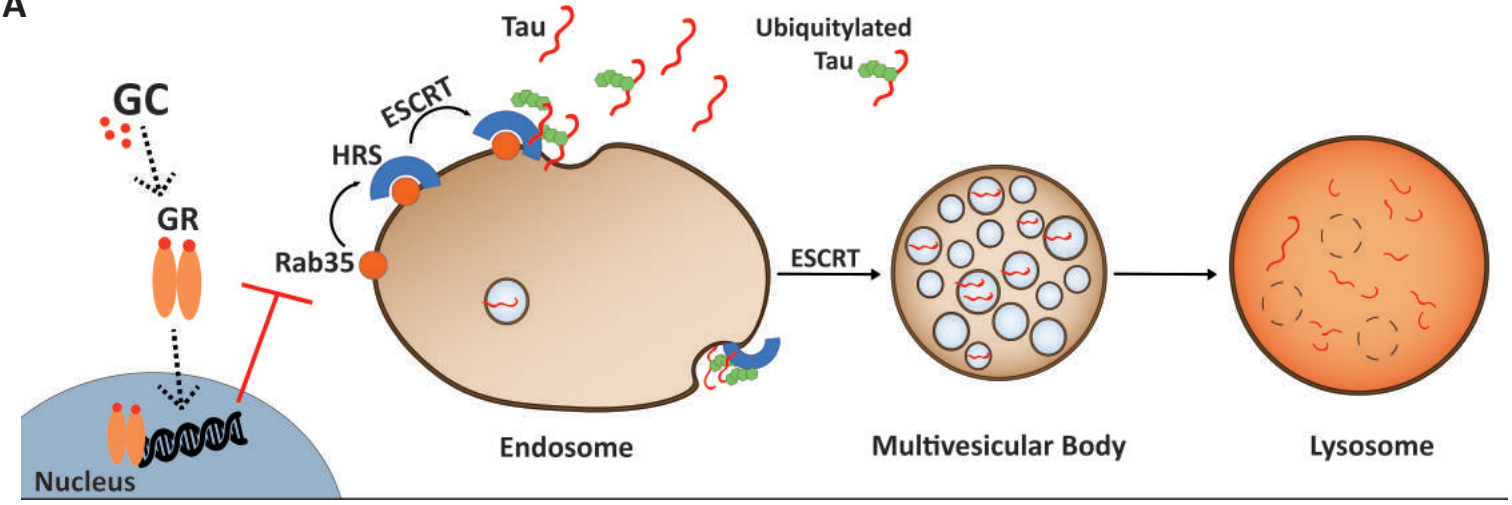
Tau
Ubiquitylated
Tau
GC
ESCRT
HRS
GR
Rab35
ESCRT
Nucleus
Endosome
Multivesicular Body
Lysosome

Table 1

Position	Chromosome	Start	End
1	chr5	115630873	115630972
2	chr5	115631594	115631675
3	chr5	115631971	115632003
4	chr5	115632442	115632541
5	chr5	115632583	115632682
6	chr5	115633507	115633606
7	chr5	115633735	115633834
8	chr5	115635642	115635723
9	chr5	115635734	115635827
10	chr5	115637535	115637616
11	chr5	115640541	115640640
12	chr5	115645909	115646008
13	chr5	115646118	115646217
14	chr5	115647366	115647465